U. S. Naval Research Laboratory
Washington, DC 20375-5320

NRL/5340/FR--2021/1

Particle Flow Solutions Avoiding Stiff Integration

David Frederic Crouse

Surveillance Technology Branch
Radar Division

May 25, 2021

REPORT DOCUMENTATION PAGE

Form Approved
OMB No. 0704-0188

1. REPORT DATE (DD-MM-YYYY)	2. REPORT TYPE	3. DATES COVERED (From – To)
25-05-2021	NRL Formal Report	

4. TITLE AND SUBTITLE

Particle Flow Solutions Avoiding Stiff Integration

5a. CONTRACT NUMBER

5b. GRANT NUMBER

5c. PROGRAM ELEMENT NUMBER
63801N

6. AUTHOR(S)

David Frederic Crouse

5d. PROJECT NUMBER

5e. TASK NUMBER

5f. WORK UNIT NUMBER
1R68

7. PERFORMING ORGANIZATION NAME(S) AND ADDRESS(ES)

Naval Research Laboratory
4555 Overlook Avenue, SW
Washington, DC 20375-5320

8. PERFORMING ORGANIZATION REPORT NUMBER

NRL/5340/FR--2021/1

9. SPONSORING / MONITORING AGENCY NAME(S) AND ADDRESS(ES)

Office of Naval Research
One Liberty Center
875 N. Randolph Street, Suite 1425
Arlington, VA 22203-1995

10. SPONSOR / MONITOR'S ACRONYM(S)
ONR

11. SPONSOR / MONITOR'S REPORT NUMBER(S)

12. DISTRIBUTION / AVAILABILITY STATEMENT
DISTRIBUTION STATEMENT A. Approved for public release: distribution unlimited.

13. SUPPLEMENTARY NOTES

14. ABSTRACT

Particle flow filters are a promising approach to nonlinear Bayesian estimation. However, the only flow with an analytic solution is the so-called "exact flow." Other flows, including the geodesic and Gromov flows, are often represented by stiff deterministic or stochastic differential equations that must be numerically integrated. In this paper, we derive an analytic solution for the geodesic flow and we reduce the Gromov flow to an explicit term plus simple integrals involving a single Wiener process. Given the analytic solutions, good asymptotic performance as a function of the measurement variance is demonstrated.

15. SUBJECT TERMS

Particle filtering, Particle flow, Bayesian estimation, Nonlinear estimation, Explicit solution, Gaussian approximation

16. SECURITY CLASSIFICATION OF:			17. LIMITATION OF ABSTRACT	18. NUMBER OF PAGES	19a. NAME OF RESPONSIBLE PERSON
a. REPORT	b. ABSTRACT	c. THIS PAGE			David F. Crouse
Unclassified	Unclassified	Unclassified	SAR	24	19b. TELEPHONE NUMBER *(Include area code)* 202-404-1859

Standard Form 298 (Rev. 8-98)
Prescribed by ANSI Std. Z39.18

This page intentionally left blank

CONTENTS

1. INTRODUCTION 1

2. THE PARTICLE FLOW FILTER WITH UPDATES IN LOCAL COORDINATES 1

3. THE GAUSSIAN GEODESIC FLOW 3
   - 3.1 One-Dimensional Linear Geodesic Case 3
   - 3.2 Two-Dimensional Linear Geodesic Case 4
   - 3.3 Higher-Dimensional Linear Geodesic Cases 5

4. THE GAUSSIAN GROMOV FLOW 6
   - 4.1 One-Dimensional Linear Gromov Case 7
   - 4.2 Two-Dimensional Linear Gromov Case 9
   - 4.3 Arbitrary-Dimensional Linear Gromov Case 11

5. SIMULATION EXAMPLE 11

6. CONCLUSION 16

REFERENCES 17

APPENDIX A—The Analytic Solution of the "Exact" Flow 19
   - A.1 The Solution Linearized Around the Prior Mean 19
   - A.2 The Solution Linearized Around Each Particle 19

PARTICLE FLOW SOLUTIONS AVOIDING STIFF INTEGRATION

1. INTRODUCTION

ORIGINALLY introduced in [1], particle flow filters (PFFs), also known as homotopy particle filters or the Daum-Huang filter, are an alternative to traditional Markov-chain Monte Carlo particle filters for nonlinear Bayesian estimation. Unlike traditional particle filters, PFFs are not subject to particle collapse and are thus more appealing. Rather than resampling particles, PFFs move particles according to a deterministic or a stochastic differential equation (the "flow"). The specific differential equation used determines the type of PFF. A key step in a PFF is the numeric integration of these differential equations.

The flow integration in PFFs can be difficult. The differential equations can be stiff, which has led to the development of a number of heuristic step-size selection algorithms, such as those in [2–6]. In can be difficult to determine whether poor performance in a PFF is due to inaccuracies in integrating the flow, or whether it is due to theoretical limitations in the flow used. An analytic solution to a flow called the "exact flow," first introduced in [7], is given in [8]. Note that two versions of the "exact flow" exist. The one of [8] utilizes a linearization around the prior distribution's mean, whereas a variant with derivations in [5, 6] utilizes a linearization about each particle. Appendix A provides both flows and demonstrates a bias present when linearizing around each particle. However, there are many more flows in existence than just the exact flow of [8], for which an analytic solution exists. For example, broad categories of flows are described in [9]. This paper seeks to find explicit solutions to more flows.

The key to obtaining the explicit flow solutions of this paper is the use of specific coordinate systems. Consequently, the assumed structure of the PFF and the assumed coordinate systems needed are described in Section 2. Two flows are chosen for explicit solution. Both are specific forms of "nonzero diffusion" filters from [10–12], which have a simple explicit form when some terms are approximated under an assumption of a Gaussian prior. In [5, 6], the unbiasedness of one such flow, the "geodesic flow," which is defined by a deterministic differential equation, is considered. In this report, an explicit solution to the geodesic flow is provided in Section 4. The second flow considered, under similar assumptions, is the Gromov flow, which is defined by a stochastic differential equation. In Section 4, it is shown that the Gromov flow reduces to a deterministic term and three integrals over a scalar Wiener process.

A simulation example considering the exact flow, the geodesic flow, and the Gromov flow is given in Section 5. The results are summarized in Section 6.

2. THE PARTICLE FLOW FILTER WITH UPDATES IN LOCAL COORDINATES

A PFF approximates a probability density function (PDF) as a set of particles that are usually unweighted. The density of the particles in a particular region is rightly representative of the uncertainty of the likelihood of a target in that region. Often, an estimate for display is obtained using the sample mean and the covariance matrix of the particles.

Manuscript approved May 25, 2021.

During a measurement update, an individual particle $\mathbf{x}$ is moved according to a stochastic differential equation of the form

$$d\mathbf{x}_\lambda = \mathbf{f}_\lambda d\lambda + \mathbf{B}_\lambda d\boldsymbol{\beta}_\lambda, \tag{1}$$

where λ is a parameter that is integrated from 0 to 1, and $d\boldsymbol{\beta}_\lambda$ is a differential Wiener process. The flow is defined by the drift $\mathbf{f}_\lambda$ and the diffusion $\mathbf{B}_\lambda$, which depend on $\mathbf{x}_\lambda$. Deterministic flows have the matrix $\mathbf{B}_\lambda = 0$.

Measurements of the form

$$\mathbf{z} = \mathbf{h}(\mathbf{x}) + \mathbf{w} \tag{2}$$

are considered, where $\mathbf{h}$ is a nonlinear function and $\mathbf{w}$ is a Gaussian random variable with covariance matrix $\mathbf{R}$. This and the sample moments of the particles suffices to define the flows considered in this paper.

Even if one wishes to perform estimation in Cartesian coordinates, the PFF need not be run in Cartesian coordinatures during measurement updates. Indeed, it was observed in [5, 6] that the filter performed better when the update is performed in a coordinate system such that the measurement is linear. For example, if one is tracking using directional measurements consisting of azimuth and elevation components, the target state could be in spherical coordinates (including range, which is not part of the measurement). The flow solutions in this paper are derived assuming that the particles have been converted to local coordinates. Thus, a measurement update step might have the following form:

1. Particles are given in Cartesian coordinates.
2. Convert the particles into a coordinate system in which the measurement is a linear function of the state. Specifically, the local measurement equation of the transformed state $\tilde{\mathbf{x}}$ is of the form

$$\mathbf{z} = \mathbf{H}\tilde{\mathbf{x}} + \mathbf{w}, \tag{3}$$

   where $\mathbf{H}$ consists only of 0s and 1s with a single 1 per row.
3. Perform the measurement update by integrating Eq. (1) with a chosen particle flow.
4. Convert the particles back to Cartesian coordinates.

Note that when dealing with directional measurements, it was observed that additional heuristics in Step 4 can improve the performance of the filter significantly. For example, when using spherical coordinates locally, performance often can be often improved significantly by taking the absolute value of the range component of the particles, because the flows sometimes can move particles to negative ranges.

In the following sections, it is assumed that all measurements are scalars. For vector measurements, this means that if the measurement covariance matrix $\mathbf{R}$ is diagonal, then each component of the vector measurement is treated as a separate independent measurement and a separate measurement update is performed for each component. Thus, if $\mathbf{z}$ is d_z-dimensional, and $\mathbf{R}$ is a diagonal matrix, the measurement

update is performed as d_z 1-dimensional measurement updates, with the ith measurement being z_i with variance $R_{k,k}$ that is the ith diagonal of $\mathbf{R}$.

If $\mathbf{R}$ is not diagonal, the measurement is transformed to diagonalize $\mathbf{R}$ and then the update is performed. That is, $\tilde{\mathbf{z}}$ is used as the measurement where

$$\tilde{\mathbf{z}} = \mathbf{V}\mathbf{z} \tag{4}$$

and $\mathbf{V}$ is the eigenvectors of $\mathbf{R}$. This means that the covariance matrix associated with $\tilde{\mathbf{z}}$ is $\mathbf{V}\mathbf{R}\mathbf{V}' = \mathbf{D}$, the diagonal matrix of eigenvalues. Note, however, that transforming the measurement in this manner affects the coordinate transformation applied to the target state in Step 1 above. Specifically, the components of the transformed state that are linear in the measurement domain also must be multiplied by $\mathbf{V}$ and, similarly, the components involved in the inverse transformation are multiplied by $\mathbf{V}'$.

For simplicity of notation, the first component of a particle in local coordinates is assumed to correspond to the component observed by the measurement during the update. When updating with a vector measurement, the indexation for additional components during the update will have to be adjusted.

3. THE GAUSSIAN GEODESIC FLOW

Originating as a nonzero diffusion flow [3, 11, 13], the geodesic flow is essentially the Gromov flow without the stochastic term. Approximating the prior distribution as a Gaussian with covariance matrix $\mathbf{P}$ (in practice, the sample covariance of the prior particles is used), the geodesic flow under the Gaussian prior approximation is given by

$$\mathbf{f}_\lambda = -\left(\mathbf{P}^{-1} + \lambda \mathbf{H}^T \mathbf{R}^{-1} \mathbf{H}\right)^{-1} \mathbf{H}^T \mathbf{R}^{-1} \left(\mathbf{h}(\mathbf{x}_\lambda) - \mathbf{z}\right) \tag{5}$$

with

$$\frac{d\mathbf{x}_\lambda}{d\lambda} = \mathbf{f}_\lambda, \tag{6}$$

where, for nonlinear problems, the matrix $\mathbf{H}$ is taken to be

$$\mathbf{H}^T = \nabla_{\mathbf{x}} \left(\mathbf{h}(\mathbf{x})\right)^T, \tag{7}$$

where $\nabla_{\mathbf{x}}$ is the gradient operator.

In the explicit solutions that follow, it is assumed that the particles have been transformed into a local coordinate system as described in Section 2 and that multivariate measurements have been transformed so that updates can be performed as sequential 1D updates.

3.1 One-Dimensional Linear Geodesic Case

In the case where the particles are one-dimensional, $\mathbf{x} = x$, the measurement function $\mathbf{h}(\mathbf{x}) = x$, and $\mathbf{H} = 1$. Assuming a Gaussian prior, the problem is just an issue of fusing two Gaussians, one with a variance

of P and another with a variance of R. In such an instance, the flow of Eq. (5) becomes

$$\frac{dx_\lambda}{d\lambda} = \frac{R^{-1}(z - x_\lambda)}{P^{-1} + \lambda R^{-1}} \tag{8}$$

$$= \frac{P(z - x_\lambda)}{R + \lambda P}. \tag{9}$$

The solution to this differential equation, taking into account the initial value of a particle x at $\lambda = 0$ as x_0, is

$$x_\lambda = \frac{Rx_0 + \lambda P z}{R + P\lambda}. \tag{10}$$

Thus, the posterior value is

$$x_1 = \frac{Rx_0 + Pz}{R + P}. \tag{11}$$

In the limit as $R \to 0$, $x_1 \to z$, and as $R \to \infty$, $x_1 \to x_0$, as one would expect.

3.2 Two-Dimensional Linear Geodesic Case

In this instance, the state $\mathbf{x}$ is a 2×1 vector, and the scalar measurement in the coordinate system of Section 2 is taken to be the first element of $\mathbf{x}$. That is

$$\mathbf{P} = \begin{bmatrix} p_{11} & p_{12} \\ p_{12} & p_{22} \end{bmatrix} \tag{12}$$

$$\mathbf{H} = \begin{bmatrix} 1 & 0 \end{bmatrix} \tag{13}$$

$$\mathbf{x} = \begin{bmatrix} x_1 \\ x_2 \end{bmatrix}. \tag{14}$$

In this instance, the differential equation for the flow becomes

$$\frac{d\mathbf{x}_\lambda}{d\lambda} = \begin{bmatrix} \dfrac{p_{11}(z - x_{1,\lambda})}{R + p_{11}\lambda} \\ \dfrac{p_{12}(z - x_{1,\lambda})}{R + p_{11}\lambda} \end{bmatrix}. \tag{15}$$

It can be seen that the differential equation for x_1 can be solved independently of that for x_2. That is,

$$\frac{dx_1}{d\lambda} = \frac{p_{11}(z - x_1)}{R + p_{11}\lambda}. \tag{16}$$

Comparing to Eq. (9) in Section 3.1, the solution for x_1, taking the initial condition into account, is

$$x_{1,\lambda} = \frac{Rx_{1,0} + \lambda p_{11} z}{R + p_{11}\lambda}. \tag{17}$$

Substituting Eq. (17) into the differential equation for $x_{2,\lambda}$ in Eq. (15) results in the differential equation

$$\frac{dx_{2,\lambda}}{d\lambda} = \frac{p_{12}\left(z - \frac{Rx_{1,0}+\lambda p_{11} z}{R+p_{11}\lambda}\right)}{R + p_{11}\lambda} \tag{18}$$

$$= \frac{p_{12} R\,(z - x_{10})}{(R + p_{11}\lambda)^2}. \tag{19}$$

The differential equation for $x_{x,\lambda}$ can just be integrated to get

$$x_{2,\lambda} = x_{2,0} + \frac{\lambda p_{12}\,(z - x_{10})}{R + p_{11}\lambda}. \tag{20}$$

Thus, an explicit solution to the entire integration over the flow is

$$\mathbf{x}_1 = \begin{bmatrix} \dfrac{Rx_{1,0} + p_{11} z}{R + p_{11}} \\ x_{2,0} + \dfrac{p_{12}\,(z - x_{10})}{R + p_{11}} \end{bmatrix}. \tag{21}$$

3.3 Higher-Dimensional Linear Geodesic Cases

When the state $\mathbf{x}$ is a 2×1 vector and the measurement is again the first component, the parameters become

$$\mathbf{P} = \begin{bmatrix} p_{11} & p_{12} & p_{13} \\ p_{12} & p_{22} & p_{23} \\ p_{13} & p_{23} & p_{33} \end{bmatrix} \tag{22}$$

$$\mathbf{H} = \begin{bmatrix} 1 & 0 & 0 \end{bmatrix} \tag{23}$$

$$\mathbf{x} = \begin{bmatrix} x_1 \\ x_2 \\ x_3 \end{bmatrix}. \tag{24}$$

The differential equation for the flow is thus

$$d\mathbf{x}_\lambda = \begin{bmatrix} \dfrac{p_{11}(z - x_{1,\lambda})}{R + p_{11}\lambda} \\ \dfrac{p_{12}(z - x_{1,\lambda})}{R + p_{11}\lambda} \\ \dfrac{p_{13}(z - x_{1,\lambda})}{R + p_{11}\lambda} \end{bmatrix} d\lambda. \tag{25}$$

The similarity to Eq. (15) in the 2D case can be seen. Again, one can solve for $x_{1,\lambda}$ and then solve for the other components. The pattern continues for higher-dimensional problems. Thus, the solution in the general d_x-dimensional case is

$$\mathbf{x}_1 = \begin{bmatrix} \dfrac{Rx_{1,0} + p_{11}z}{R + p_{11}} \\ x_{2,0} + \dfrac{p_{12}\,(z - x_{10})}{R + p_{11}} \\ x_{3,0} + \dfrac{p_{13}\,(z - x_{10})}{R + p_{11}} \\ \vdots \\ x_{d_x,0} + \dfrac{p_{1d_x}\,(z - x_{10})}{R + p_{11}} \end{bmatrix}. \tag{26}$$

4. THE GAUSSIAN GROMOV FLOW

Whereas the geodesic flow was derived assuming a stochastic differential equation of the form in Eq. (1), it omitted the diffusion term. The Gromov flow includes the diffusion term. Specifically, the explicit solution of [10] under the approximation of a scalar distribution in local coordinates is used. A summary of the literature and a full derivation is given in [6].

The Gromov flow used here is

$$\mathbf{f}_\lambda = -\left(\mathbf{P}^{-1} + \lambda \mathbf{H}^T \mathbf{R}^{-1} \mathbf{H}\right)^{-1} \mathbf{H}^T \mathbf{R}^{-1} \left(\mathbf{h} - \mathbf{z}\right) \tag{27}$$

$$\mathbf{Q}_\lambda = \left(\mathbf{P}^{-1} + \lambda \mathbf{H}^T \mathbf{R}^{-1} \mathbf{H}\right)^{-1} \mathbf{H}^T \mathbf{R}^{-1} \mathbf{H} \left(\mathbf{P}^{-1} + \lambda \mathbf{H}^T \mathbf{R}^{-1} \mathbf{H}\right)^{-1}, \tag{28}$$

where $\mathbf{Q}_\lambda$ is the square of the diffusion matrix in Eq. (1)

$$\mathbf{Q}_\lambda = \mathbf{B}_\lambda \mathbf{B}_\lambda^T. \tag{29}$$

The diffusion matrix $\mathbf{B}_\lambda$ can be obtained analytically. If $\mathbf{S}_R$ is a matrix, such as a Cholesky decomposition of $\mathbf{R}$, that satisfies

$$\mathbf{R} = \mathbf{S}_R \mathbf{S}_R^T, \tag{30}$$

then

$$\mathbf{B}_\lambda = \left(\mathbf{P}^{-1} + \lambda \mathbf{H}^T \mathbf{R}^{-1} \mathbf{H}\right)^{-1} \mathbf{H}^T \left(\mathbf{S}_R^T\right)^{-1}. \tag{31}$$

When the measurement $\mathbf{z}$ is a scalar, the Wiener process $\boldsymbol{\beta}_\lambda$ in Eq. (1) is scalar.

In the explicit solutions that follow, it is assumed that the particles have been transformed into a local coordinate system as described in Section 2 and that multivariate measurements have been transformed so that updates can be performed as sequential 1D updates.

4.1 One-Dimensional Linear Gromov Case

A scalar state $\mathbf{x} = x$ in the coordinate system of Section 2 initially is used with a measurement function $\mathbf{h}(\mathbf{x}) = x$, so that $\mathbf{H} = 1$. The standard deviation of the measurement is $S = \sqrt{R}$. In such an instance, the stochastic differential equation Eq. (1) takes the form

$$dx_t = (a(t)x_t + b(t))\, dt + c(t) d\beta_t, \tag{32}$$

where

$$a(t) = -\frac{P}{S^2 + Pt} \tag{33}$$

$$b(t) = \frac{Pz}{S^2 + Pt} \tag{34}$$

$$c(t) = \frac{PS}{S^2 + Pt}. \tag{35}$$

An explicit solution for an Ito integral of such a stochastic differential equation from time $t = 0$ to $t = \lambda$ is given in [14, Ch. 4.4] as

$$x_\lambda = \Phi_\lambda \left(x_0 + \int_0^\lambda \Phi_t^{-1} b(t) dt + \int_0^\lambda \Phi_t^{-1} c(t) d\beta_t\right) \tag{36}$$

$$\Phi_\lambda = \exp\left(\int_0^\lambda a(t) dt\right). \tag{37}$$

In this instance,

$$\Phi_\lambda = \exp\left(-\int_0^\lambda \frac{P}{S^2+Pt}dt\right) \tag{38}$$

$$= \exp\left(\log\left(S^2\right) - \log\left(S^2+P\lambda\right)\right) \tag{39}$$

$$= \frac{S^2}{S^2+P\lambda} \tag{40}$$

and

$$\Phi_t^{-1} b(t) = \frac{Pz}{S^2} \tag{41}$$

$$\Phi_t^{-1} c(t) = \frac{P}{S}, \tag{42}$$

so Eq. (36) becomes

$$x_\lambda = \frac{S^2 x_0 + Pz\lambda}{S^2+P\lambda} + \frac{PS}{S^2+P\lambda}\int_0^\lambda d\beta_t \tag{43}$$

with

$$\int_0^\lambda d\beta_t \sim \mathcal{N}\left\{0,\lambda\right\}. \tag{44}$$

Consequently, at $\lambda = 1$,

$$x_1 \sim \mathcal{N}\left\{\frac{Rx_0+Pz}{R+P}, \frac{P^2R}{(R+P)^2}\right\}. \tag{45}$$

Note that each particle being propagated should be drawn independently. As $R \to 0$, the mean goes to z and the variance goes to 0, as might be expected. Similarly, as $R \to \infty$, the mean goes to x_0, and the variance also goes to 0, as would also be expected.

4.2 Two-Dimensional Linear Gromov Case

In this instance, the state $\mathbf{x}$ is a 2×1 vector, and the measurement observed is the first element of the state, so

$$\mathbf{P} = \begin{bmatrix} p_{11} & p_{12} \\ p_{12} & p_{22} \end{bmatrix} \tag{46}$$

$$\mathbf{H} = \begin{bmatrix} 1 & 0 \end{bmatrix} \tag{47}$$

$$\mathbf{x} = \begin{bmatrix} x_1 \\ x_2 \end{bmatrix}, \tag{48}$$

with $\mathbf{h}(\mathbf{x}) = x_1$. This leads to Eq. (27) and Eq. (31) becoming

$$\mathbf{f}_\lambda = -\begin{bmatrix} \frac{p_{11}x_{1,\lambda}}{S^2 + p_{11}\lambda} \\ \frac{p_{12}x_{1,\lambda}}{S^2 + p_{11}\lambda} \end{bmatrix} + \begin{bmatrix} \frac{p_{11}z}{S^2 + p_{11}\lambda} \\ \frac{p_{12}z}{S^2 + p_{11}\lambda} \end{bmatrix} \tag{49}$$

$$\mathbf{B}_\lambda = \begin{bmatrix} \frac{p_{11}S}{S^2 + p_{11}\lambda} \\ \frac{p_{12}S}{S^2 + p_{11}\lambda} \end{bmatrix} \tag{50}$$

$$d\mathbf{x}_\lambda = \mathbf{f}_\lambda d\lambda + \mathbf{B}_\lambda d\beta_\lambda. \tag{51}$$

It can be seen that the solution for $x_{1,\lambda}$ is independent of that of $x_{2,\lambda}$. Thus, from Eq. (43),

$$x_{1,\lambda} = \frac{S^2 x_{1,0} + p_{11} z\lambda}{S^2 + p_{11}\lambda} + \frac{p_{11}S}{S^2 + p_{11}\lambda} \int_0^\lambda d\beta_t. \tag{52}$$

Substituting the above into the equation for the $dx_{2,\lambda}$ component of Eq. (51) results in

$$dx_{2,\lambda} = \left(-p_{12} \left(\frac{S^2 x_{1,0} + p_{11} z\lambda}{\left(S^2 + p_{11}\lambda\right)^2} + \frac{p_{11}S}{\left(S^2 + p_{11}\lambda\right)^2} \int_0^\lambda d\beta_t \right) + \frac{p_{12}z}{S^2 + p_{11}\lambda} \right) d\lambda + \frac{p_{12}S}{S^2 + p_{11}\lambda} d\beta_\lambda \tag{53}$$

$$= \left(\frac{p_{12}z}{S^2 + p_{11}\lambda} - \frac{p_{12}\left(S^2 x_{1,0} + p_{11} z\lambda\right)}{\left(S^2 + p_{11}\lambda\right)^2} - \frac{p_{12}p_{11}S}{\left(S^2 + p_{11}\lambda\right)^2} \int_0^\lambda d\beta_t \right) d\lambda + \frac{p_{12}S}{S^2 + p_{11}\lambda} d\beta_\lambda. \tag{54}$$

Since no $x_{2,\lambda}$ terms appear in the above, the individual terms can just be integrated to get

$$x_{2,\lambda} = x_{2,0} + \frac{p_{12}(z - x_{10})\lambda}{S^2 + p_{11}\lambda} - p_{12}p_{11}S \int_0^\lambda \frac{1}{\left(S^2 + p_{11}s\right)^2} \int_0^s d\beta_t ds + p_{12}S \int_0^\lambda \frac{1}{S^2 + p_{11}t} d\beta_t. \tag{55}$$

The second stochastic integral evaluates to

$$\int_0^{\lambda} \frac{1}{S^2 + p_{11}t} d\beta_t \sim \mathcal{N}\left\{0, \frac{1}{S^2 + p_{11}\lambda}\right\}. \tag{56}$$

However, the solution to the first integral is not found as easily. Moreover, because all integrals are integrating over the same Wiener process, the integral values are correlated and must be found jointly. Thus, two possible approximation methods are suggested:

1. Discard the integral terms in Eq. (55) and simulate the Wiener integral in Eq. (52), by sampling the $\mathcal{N}\{0, \lambda\}$ distribution.

2. Generate all of the integral values by simulating a scalar Wiener process and summing the discretized results to approximate the integrals. It was observed that typically, a large number of discretized steps are needed, perhaps on the order of 10^5, to model these integrals accurately without introducing instability that can affect the particles adversely compared to the above method.

The discrete approximation of stochastic integrals is discussed in [14]. All integrals are to be evaluated using N discretized steps. This will require a realization of the Wiener process β at $N+1$ times. Specifically, $t_0 = 0$, $t_N = \lambda$, and in between $t_k = (k/N)\lambda$. Let β_k denote the realization of β at the discrete time k, which corresponds to time t_k. Define

$$\Delta = (1/N)\lambda. \tag{57}$$

A simulated realization of β_k values is obtained recursively as

$$\beta_0 = 0 \tag{58}$$

$$\beta_k = \beta_{k-1} + \mathcal{N}\{0, \Delta\}. \tag{59}$$

The value β_N is the solution to the integral in Eq. (52).

For a function f, a discretization of an Ito integral over the function is

$$\int_0^{\lambda} f(t) d\beta_t \approx \sum_{k=0}^{N-1} f(t_k)\left(\beta_{k+1} - \beta_k\right). \tag{60}$$

Similarly, when given a non-random measure, an integral can be approximated with a Riemann sum as

$$\int_0^{\lambda} f(t) dt \approx \sum_{k=0}^{N-1} f(t_k)\Delta. \tag{61}$$

Combining Eq. (60) and Eq. (61) leads to the joint discretization

$$\int_0^{\lambda} f(t) \int_0^{t} d\beta_s dt \approx \sum_{k=0}^{N-1} f(t_k) \int_0^{t_k} d\beta_s \Delta \tag{62}$$

$$\approx \sum_{k=0}^{N-1} \Delta f(t_k) \sum_{j=0}^{k-1} \left(\beta_{j+1} - \beta_j\right) \tag{63}$$

$$= \sum_{k=0}^{N-1} \Delta f(t_k) \left(\beta_k - \beta_0\right). \tag{64}$$

4.3 Arbitrary-Dimensional Linear Gromov Case

As was the case for the geodesic flow, when considering the Gromov flow, in higher dimensions, all subsequent dimensions are only coupled to the first dimension. Thus, the solution from Section 4.2 generalizes to an arbitrary number of dimensions as

$$\mathbf{x}_1 = \begin{bmatrix} \dfrac{S^2 x_{1,0} + p_{11} z}{S^2 + p_{11}} + \dfrac{p_{11} S}{S^2 + p_{11}} \displaystyle\int_0^1 d\beta_t \\ x_{2,0} + \dfrac{p_{12}(z - x_{10})}{S^2 + p_{11}} - p_{12} p_{11} S \displaystyle\int_0^1 \frac{1}{\left(S^2 + p_{11} s\right)^2} \int_0^s d\beta_t ds + p_{12} S \int_0^1 \frac{1}{S^2 + p_{11} t} d\beta_t \\ \vdots \\ x_{d_x,0} + \dfrac{p_{1d_x}(z - x_{10})}{S^2 + p_{11}} - p_{1d_x} p_{11} S \displaystyle\int_0^1 \frac{1}{\left(S^2 + p_{11} s\right)^2} \int_0^s d\beta_t ds + p_{1d_x} S \int_0^1 \frac{1}{S^2 + p_{11} t} d\beta_t \end{bmatrix}. \tag{65}$$

The same stochastic integrals are present in all dimensions after the first one, so the computational complexity of the integration does not increase as the dimensionality of the problem increases.

5. SIMULATION EXAMPLE

As an example, the fusion of a single time-difference-of-arrival (TDOA) measurement with a Gaussian prior distribution in two dimensions is considered. The PDF of the TDOA measurement is extremely nonlinear in Cartesian coordinates. In order to use the algorithm developed in this paper, one must determine an invertible transformation between Cartesian coordinates and a coordinate system where the TDOA measurement is a component of the state. Ideally, the coordinate system will be fully bijective. However, without having an obvious systematic approach to generate such a transformation, a coordinate system of a TDOA measurement and a polar angle is chosen.

A conversion from such TDOA-polar coordinate systems into Cartesian coordinates is needed. This can be derived in a similar manner to the bistatic conversions utilizing direction cosines that are in [15]. The geometry of the problem is illustrated in Fig. 1. Assuming a constant index of refraction, the measured

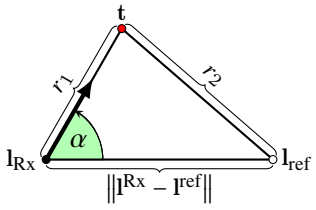

Fig. 1—The geometry used in the coordinate systems with TDOA measurements. The target and emitter are at $\mathbf{t}$. The reference receiver $\mathbf{l}_{\text{ref}}$ determines the reference time of arrival of the signal that the time at receiver $\mathbf{l}_{\text{Rx}}$ is differenced with. The arrow is the direction of a unit-vector $\mathbf{u}$ from the non-reference receiver to the target.

TDOA is expressed as

$$\text{TDOA} = \frac{1}{c}\left(\|\mathbf{t} - \mathbf{l}_{\text{Rx}}\| - \|\mathbf{t} - \mathbf{l}_{\text{ref}}\|\right) \tag{66}$$

where c is the speed of signal propagation. For simplicity, it is assumed that c has been multiplied out and there is a range difference of

$$\begin{aligned} r_{\text{diff}} &= \|\mathbf{t} - \mathbf{l}_{\text{Rx}}\| - \|\mathbf{t} - \mathbf{l}_{\text{ref}}\| && (67)\\ &= r_1 - r_2. && (68) \end{aligned}$$

Let $\mathbf{u}$ be a unit vector pointing from the receiver at $\mathbf{l}_{\text{Rx}}$ to the target. The location of the target is given by

$$\mathbf{t} = \mathbf{l}_{\text{Rx}} + r_1\mathbf{u}. \tag{69}$$

To solve for r_1 given r_{diff} and $\mathbf{u}$, note that the dot product of the target location and the vector between the receivers is

$$r_1\mathbf{u}^T\left(\mathbf{l}_{\text{ref}} - \mathbf{l}_{\text{Rx}}\right) = r_1\|\mathbf{l}_{\text{ref}} - \mathbf{l}_{\text{Rx}}\|\cos(\alpha) \tag{70}$$

where the angle α is the angle between the $\mathbf{u}$ and $\mathbf{l}_{\text{ref}} - \mathbf{l}_{\text{Rx}}$ vectors. Using the law of cosines on the triangle in Fig. 1 and then substituting Eq. (70) leads to the relation

$$\begin{aligned} r_2^2 &= r_1^2 + \|\mathbf{l}_{\text{ref}} - \mathbf{l}_{\text{Rx}}\|^2 - 2r_1\|\mathbf{l}_{\text{ref}} - \mathbf{l}_{\text{Rx}}\|\cos(\alpha) && (71)\\ &= r_1^2 + \|\mathbf{l}_{\text{ref}} - \mathbf{l}_{\text{Rx}}\|^2 - 2r_1\mathbf{u}^T\left(\mathbf{l}_{\text{ref}} - \mathbf{l}_{\text{Rx}}\right). && (72) \end{aligned}$$

Using Eq. (68), the range r_2 is expressed as

$$r_2 = r_1 - r_{\text{diff}}. \tag{73}$$

Substituting into Eq. (72), results in

$$r_1 = \frac{r_{\text{diff}}^2 - \|\mathbf{l}_{\text{ref}} - \mathbf{l}_{\text{Rx}}\|^2}{2\left(r_{\text{diff}} - \mathbf{u}^T\left(\mathbf{l}_{\text{ref}} - \mathbf{l}_{\text{Rx}}\right)\right)}. \tag{74}$$

Substituting into Eq. (69), the conversion from r_{diff} and $\mathbf{u}$ to Cartesian coordinates is

$$\mathbf{t} = \mathbf{l}_{\text{Rx}} + \frac{r_{\text{diff}}^2 - \|\mathbf{l}_{\text{ref}} - \mathbf{l}_{\text{Rx}}\|^2}{2\left(r_{\text{diff}} - \mathbf{u}^T\left(\mathbf{l}_{\text{ref}} - \mathbf{l}_{\text{Rx}}\right)\right)}\mathbf{u}. \tag{75}$$

To complete the definition of the TDOA-polar coordinate system, the unit vector $\mathbf{u}$ is defined as

$$\mathbf{u} = \begin{bmatrix} \cos(\theta) \\ \sin(\theta) \end{bmatrix}. \tag{76}$$

In the inverse direction, this means that

$$\theta = \arctan 2\left(y, x\right). \tag{77}$$

Note that the transformation from Cartesian to TDOA-polar as defined thus far is one-to-one. However, it is not mathematically "onto." Points that are not included in the forward conversion are those such that r_1 in Eq. (74) is negative. The PFF can possibly move points to a region where r_1 is negative. In such an instance, it was found that for $r_1 < 0$, changing Eq. (69) to the heuristic

$$\mathbf{t} = \mathbf{l}_{\text{ref}} - r_1\mathbf{u} \tag{78}$$

works well.

In the scenario considered, a reference sensor is placed at $\mathbf{l}_{\text{ref}} = [-3\,\text{km}, 0\,\text{km}]^T$ and the other sensor at $\mathbf{l}_{\text{Rx}} = [3\,\text{km}, 0\,\text{km}]^T$. The target is located at $\mathbf{x} = [4\,\text{km}, 4\,\text{km}]^T$. The measurement is taken as a range difference (already divided by c for the TDOAs). The measurement standard deviation is $200\,\text{m}$. The prior distribution is Gaussian with a mean of $\mathbf{x}_{\text{prior}} = [5\,\text{km}, 3\,\text{km}]^T$ and a diagonal covariance matrix with values of $10\,\text{km}^2$ on the diagonal in x and y.

The PFF was initialized by drawing 300 random samples from the prior distribution. The mean and covariance of the prior used in the filter was set to the sample mean and covariance of the particles, not the true values. The exact flow was implemented using the expressions of [8], which are repeated in Appendix A.1. The results of running each of the filters in this paper are shown in Fig. 2. The "Heuristic Gromov Flow" omits simulating the stochastic integrals in the cross terms (i.e. Eq. (55)) and it simulates the stochastic integral in Eq. (52) by drawing from a Gaussian distribution with zero mean and unit variance. The "Gromov Flow" simulates all integrals by generating a Wiener process with 10^5 steps. In all instances, the measurement was taken to be at the true position.

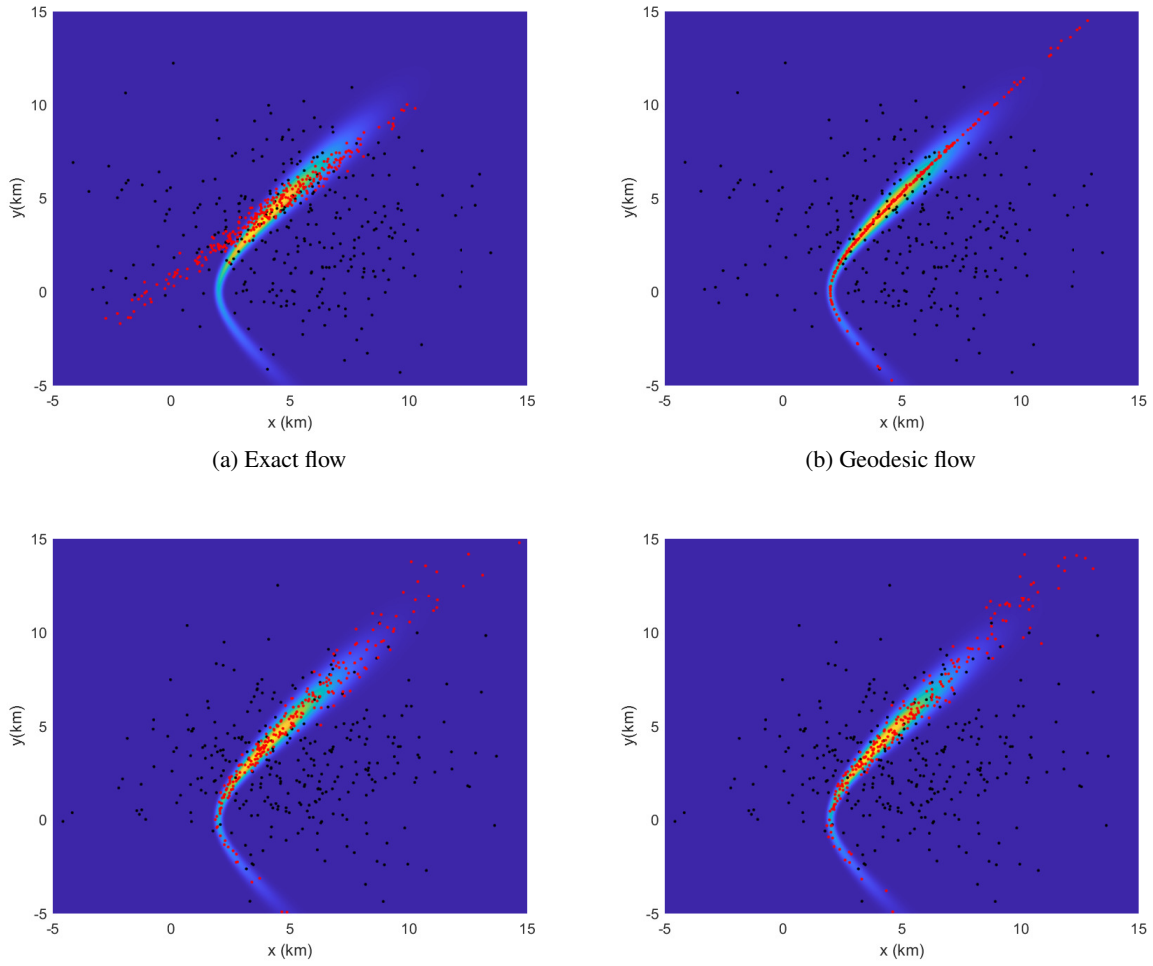

(a) Exact flow

(b) Geodesic flow

(c) Gromov flow

(d) Heuristic Gromov flow

Fig. 2—The true posterior PDF is illustrated in color below each image for the first scenario. The prior points are in black. The posterior points are in red.

It can be seen that the exact flow cannot model any of the curvature of the PDF. The geodesic flow captures the curvature, but not the spread, and each of the Gromov flows captures the curvature and spread of the PDF. However, the Gromov flows have a number of points that are rather far off, which correspond to distance points along the measurement PDF. It was observed that this significantly biases the posterior mean.

Not illustrated is the fact that the output of the flows, except for the exact flow, had a few very distant outlying points that are outside of the plotted region. These are most likely explained by the fact that the measurement PDF itself has infinitely long tails. The extent to which any of those arise in the posterior depends on how fast the prior PDF decreases. Examining Eq. (75), it can be seen that if $r_{\text{diff}} = \|\mathbf{l}_{\text{ref}} - \mathbf{l}_{\text{Rx}}\|$, there will exist a $\mathbf{u}$ such that the denominator goes to zero and $\mathbf{t}$ diverges. The presence of outliers implies that evaluation of the mean and covariance matrix would be performed best using a robust estimation algorithm, such as the blocked adaptive computationally efficient outlier nominators (BACON) algorithm of [16].

Though the exact flow is not particularly bad in Fig. 2, it can produce very bad results when the mean of the prior is not near a high-probability region of the measurements. Moving the prior mean to $\mathbf{x}_{\text{prior}} = [-5\,\text{km}, -3\,\text{km}]^T$, provides the results in Fig. 3, where the particles in the exact flow are not representative of the uncertainty in the posterior PDF.

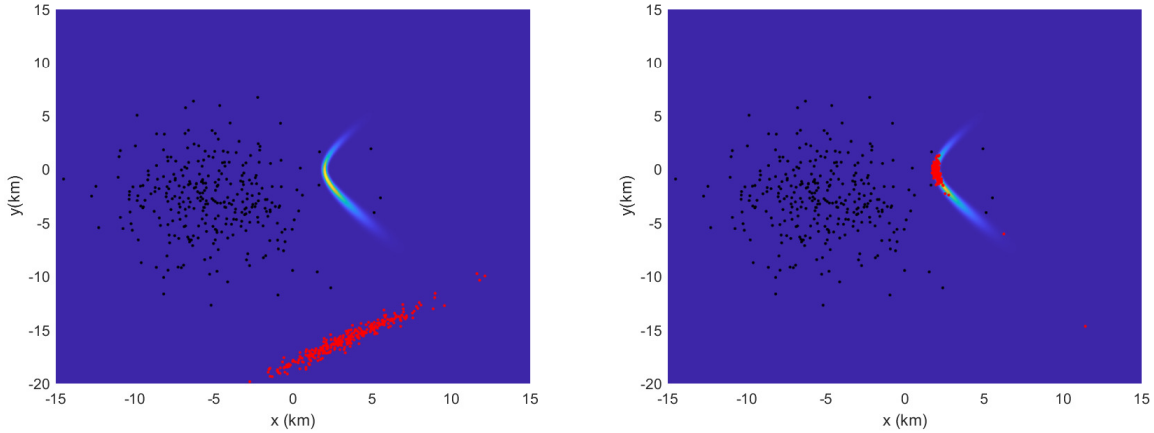

(a) Exact flow (b) Gromov flow

Fig. 3—The true posterior PDF is illustrated in color below each image for the second scenario, for which the mean of the prior distribution is rather far from the target location. The prior points are in black. The posterior points are in red.

Finally, the Gromov and geodesic flows are limited when the prior distribution is not Gaussian. Taking the first example with $\mathbf{x}_{\text{prior}} = [5\,\text{km}, 3\,\text{km}]^T$, a second measurement where the receiver is placed at $\mathbf{l}_{\text{Rx}} = [3\,\text{km}, 0\,\text{km}]^T$ is fused. The fusion of multiple TDOA measurements has been considered for cell phone localization to satisfy regulations imposed for the E911 standard [17]. The outputs of the Gromov and Geodesic flows are shown in Figs. 4a and 4c. Both have long tails that are not representative of the true distribution. However, it was noticed in simulations that given enough measurements, the Gromov flow generally will converge to a useful estimate. Thus, simply repeatedly updating the Gromov and geodesic flows over the same set of measurements was considered to see if they would tend to converge to the maximum-likelihood estimate. As seen in Figs. 4b and 4d, this appears to be the case. A direction of future research could be to determine the convergence criteria and stability to determine whether iterated particle filtering could be a useful tool for global maximum-likelihood optimization.

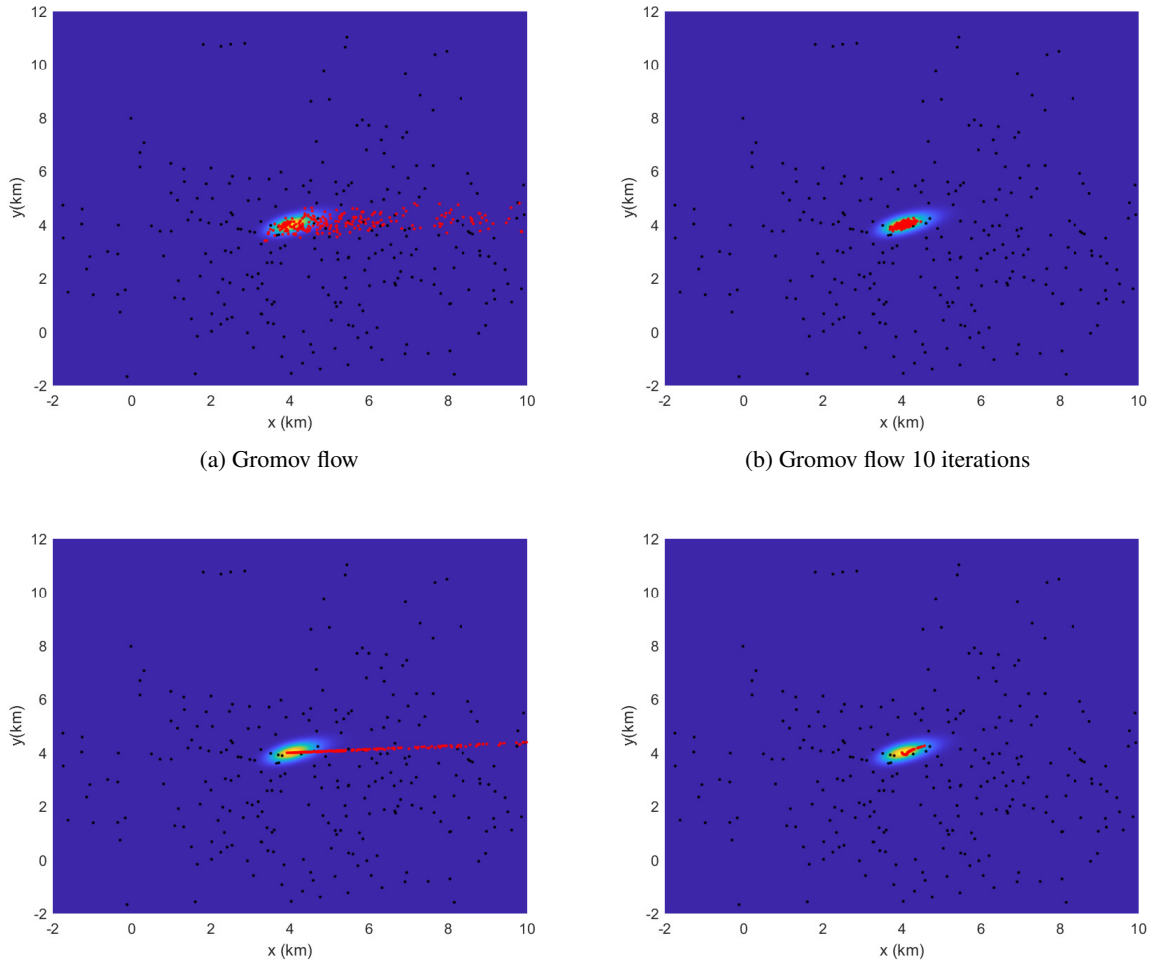

(a) Gromov flow

(b) Gromov flow 10 iterations

(c) Geodesic flow

(d) Geodesic flow 10 iterations

Fig. 4—In 4a and 4c, the true posterior PDF is shown below the prior particles (black) and posterior particles (red) after updating with two measurements. In 4b and 4d, the posterior PDF given a diffuse prior is shown with the particles after iterating the updates.

6. CONCLUSION

This paper provided an explicit solution to the geodesic flow, a solution to the Gromov flow that is expressed in terms of three stochastic integrals, and a much simpler and faster approximation to the Gromov flow that requires the simulation of a Wiener process to evaluate. By eliminating the need to evaluate stiff differential equations, the performance of the flows now can be analyzed without ambiguity whether poor performance might be due to the flow, itself, or due to an inability to integrate stiff differential equations.

The performance of both Gromov flow variants was very similar. The geodesic flow lacked the spread of the Gromov flow. All three of those flows outperformed the exact flow, which can produce very bad results when given a poor prior distribution. When the prior distribution is not Gaussian, the Gromov flow can produce poor results. However, when fusing measurements in a TDOA localization scenario, as

might be representative of what cell phone providers perform for the E911 service, it was observed that when iterating the Gromov flow over the same set of measurements, the particles tend to converge near the maximum-likelihood estimates (when given an uninformative prior).

A challenge is choosing a good coordinate system for the flow. Ideally, one should have a fully bijective coordinate system. However, in the coordinate system chosen for TDOA measurement processing, a heuristic for handling the conversion when particles move into an invalid region worked well.

REFERENCES

1. F. Daum and J. Huang, "Nonlinear Filters with Log-Homotopy," Proceedings of the SPIE: Signal and Data Processing of Small Targets, volume 6699, San Diego, CA, 26 Aug. 2007.

2. F. Daum and J. Huang, "Seven Dubious Methods to Mitigate Stiffness in Particle Flow with non-zero Diffusion for Nonlinear Filters, Bayesian Decisions, and transport," Proceedings of the SPIE: Signal and Data Processing of Small Targets, volume 9092, Baltimore, MD, 13 June 2014.

3. F. Daum and J. Huang, "Particle Flow with Non-Zero Diffusion for Nonlinear Filters, Bayesian Decisions and Transport," Proceedings of the SPIE: Signal and Data Processing of Small Targets, volume 8857, San Diego, CA, 30 Sept. 2013.

4. S. Mori, F. Daum, and J. Douglas, "Adaptive Step Size Approach to Homotopy-Based Filtering Bayesian Update," Proceedings of the 19th International Conference on Information Fusion, Heidelberg, Germany, 5–8 July 2016.

5. D. F. Crouse, "Particle Flow Filters: Biases and Bias Avoidance," Proceedings of the 22nd International Conference on Information Fusion, Ottawa, Canada, 2–5 July 2019.

6. D. F. Crouse and C. T. Lewis, "Consideration of Particle Flow Filter Implementations and Biases," NRL/MR/5344–19-9938, Naval Research Laboratory, Washington, D.C., 11 Feb. 2020.

7. D. F., J. Huang, and A. Noushin, "Exact Particle flow for Nonlinear Filters **7697** (27 Apr. 2010).

8. K. L. Bell and L. D. Stone, "Implementation of the Homotopy Particle Filter in the JPDA and MAP-PF Multi-Target Tracking Algorithms," Proceedings of the 17th International Conference on Information Fusion, Salamanca, Spain, 7–10 July 2014.

9. L. Dai and F. E. Daum, "A New Parameterized Family of Stochastic particle Flow Filters," *ArXiv* (18 Mar. 2021). URL `https://arxiv.org/abs/2103.09676`.

10. F. Daum, J. Huang, and A. Noushin, "Gromov's Method for Bayesian Stochastic particle Flow: A Simple Eact Formula for Q," Proceedings of the International Conference on Multisensor Fusion and Integration for Intelligent Systems, Bade-Baden, Germany, 19–21 Sept. 2016, pp. 540–545.

11. F. Daum and J. Huang, "Particle Flow with Non-Zero Diffusion for Nonlinear Filters," Proceedings of the SPIE: Signal Processing, Sensor Fusion, and Target Recognition XXII, Baltimore, MD, 23 May 2013.

12. F. Daum, J. Huang, and A. Noushin, "New Theory and Numerical Results from Gromov's Method for Stochastic Particle Flow Filters," Proceedings of the 21st International Conference on Information Fusion, Cambridge, UK, 10–13 July 2018.

13. F. Daum and J. Huang, "How to Avoid Normalization of Particle Flow for Nonlinear Filters: Bayesian Decisions and Transport," Proceedings of the SPIE: Signal and Data Processing of Small targets, volume 9092, Baltimore, MD, 13 June 2014.

14. P. E. Kloeden and E. Platen, *Numeric Solution of Stochastic Differential Equations* (Springer, Berlin, 1999).

15. D. F. Crouse, "Basic Tracking Using Nonlinear 3D Monostatic and Bistatic Measurements," *IEEE Aerospace and Electronic Systems Magazine* **29**(8), 4–53 (Aug. 2014).

16. N. Billor, A. S. Hadi, and P. F. Velleman, "BACON: Blocked adaptive computationally efficient outlier nominators," *Computational Statistics and Data Analysis* **34**(3), 279–298 (28 Sept. 2000).

17. J. O'Conner, B. Alexander, and E. Schorman, "CDMA Infrastructure-Based Location Finding for E911," Proceedings of the 49th IEEE Vehicular Technology Conference, Houston, TX, 16–20 May 1999, pp. 1973–1978.

18. M. A. A. Khan, *Nonlinear filtering based on log-homotopy particle flow*, PhD thesis (Rheinischen Friedrich-Wilhelms-Universität Bonn, Bonn, Germany, Aug. 2018).

Appendix A

THE ANALYTIC SOLUTION OF THE "EXACT" FLOW

A.1 The Solution Linearized Around the Prior Mean

The explicit solution to the "exact" flow as given in [8] is

$$\mathbf{x}_1 = \left(\mathbf{P}_+\mathbf{P}^{-1}\right)^{\frac{1}{2}}(\mathbf{x}_0 - \hat{\mathbf{x}}) + \hat{\mathbf{x}} + \mathbf{K}(\mathbf{z} - \mathbf{H}\hat{\mathbf{x}}) \tag{A1}$$

$$\mathbf{P}_+ = \mathbf{P} - \mathbf{KHP} \tag{A2}$$

$$\mathbf{K} = \mathbf{PH}'(\mathbf{HPH}' + \mathbf{R})^{-1} \tag{A3}$$

where $\hat{\mathbf{x}}$ and $\mathbf{P}$ are the mean and the covariance matrix of the prior distribution, $\mathbf{x}_0$ is the original position of a particle, and $\mathbf{x}_1$ is the position of the particle after the update.

To examine possible biases in this flow, the case of a scalar state with $\mathbf{H} = 1$ is considered again. The flow expression above simplifies to

$$x_1 = \sqrt{\frac{R}{P+R}}(x_0 - \hat{x}) + \hat{x} + \frac{P(z-\hat{x})}{P+R}. \tag{A4}$$

For the asymptotic values of $R \to 0$ and $R \to \infty$, $x_1 \to z$ and $x_1 \to x_0$, respectively, as would be expected.

A.2 The Solution Linearized Around Each Particle

In the literature, it is also common to derive the exact flow linearized around each particle rather than around the mean on the prior distribution. Derivations of the flow, itself, are given in [6] and [18]. However, it does not appear that anyone has derived an explicit form of the exact flow as linearized around each particle. That shall be done here for the scalar case and the bias in this version of the flow shall be revealed.

The differential equation for the exact flow derived as linearized around each particle is

$$\frac{d\mathbf{x}_\lambda}{d\lambda} = \mathbf{A}_\lambda\mathbf{x}_\lambda + \mathbf{b}_\lambda \tag{A5}$$

$$\mathbf{A}_\lambda = -\frac{1}{2}\mathbf{PH}^T\left(\lambda\mathbf{HPH}^T + \mathbf{R}\right)^{-1}\mathbf{H} \tag{A6}$$

$$\mathbf{b} = (\mathbf{I} + 2\lambda\mathbf{A})\left(\mathbf{A}\hat{\mathbf{x}}_{\text{pred}} - \left(\mathbf{PH}^T\mathbf{R}^{-1} + \lambda\mathbf{APH}^T\mathbf{R}^{-1}\right)(\mathbf{h}(\mathbf{x}) - \mathbf{z})\right). \tag{A7}$$

Considering the 1D linear case as before, $\mathbf{H} = 1$ and $\mathbf{h}(\mathbf{x}) = x$, so the above differential equation becomes

$$\frac{dx_\lambda}{d\lambda} = \frac{P(P(z-2x)\lambda - R(3x + \hat{x}_{\text{pred}} - 2z))}{2(R + P\lambda)^2}. \tag{A8}$$

The solution to this differential equation, taking into account an initial value of x_0, is

$$x_\lambda = \frac{z}{2} + \frac{R}{4(R+P\lambda)}\left(\exp\left(\frac{R}{2(R+P\lambda)}\right)\left(\frac{4x_0 - 2z}{\sqrt{e}} + \left(-2\hat{x}_{\text{pred}} + z\right)\text{Ei}\left(-\frac{1}{2}\right) + \left(2\hat{x}_{\text{pred}} - z\right)\text{Ei}\left(-\frac{R}{2(R+P\lambda)}\right)\right)\right), \tag{A9}$$

where Ei is the exponential integral function

$$\text{Ei}\,(z) \triangleq \int_{-z}^{\infty} \frac{e^{-t}}{t}\,dt. \tag{A10}$$

When $\lambda = 1$, the limit at $R \to 0$ is $x_1 = z/2$, and the limit as $R \to \infty$ is $x_1 = x_0$. Consequently, the flow is biased toward zero. It does not converge to the true solution when given a noise-free measurement, and thus, this is not a good flow to use.